Tectonophysics
September 2014, Volume 630, Pages 236-250
http://dx.doi.org/10.1016/j.tecto.2014.05.026

LiDAR offshore structural mapping and U/Pb zircon/monazite dating of Variscan strain in the Leon metamorphic domain, NW Brittany

Bernard Le Gall[a, *], Christine Authemayou[a], Axel Ehrhold[b], Jean-Louis Paquette[c], Denise Bussien[a], Gilles Chazot[a], Arthur Aouizerat[a], Yves Pastol[d]

[a] UMR/CNRS6538, Domaines Océaniques, Institut Universitaire Européen de la Mer, Place Nicolas Copernic, 29280 Plouzané, France
[b] Unité de recherche GM, Laboratoire Environnements Sédimentaires, Ifremer Centre de Bretagne, 29280 Plouzané, France
[c] Laboratoire Magmas & Volcans, UMR6524 CNRS et Université B. Pascal, 5, rue Kessler, 63038 Clermont-Ferrand, France
[d] Service Hydrographique et Oceanographique de la Marine, rue du Chatellier, 29228 Brest

*: Corresponding author : Bernard Le Gall, tel.: + 33 2 98 49 87 56 ; email address : blegall@univ-brest.fr

Abstract:

An exceptional structural picture of the immerged Variscan basement, offshore the Leon metamorphic domain, is supplied by high-resolution LiDAR and echosounder data recorded in the Molene archipelago, western Brittany (France). Various types of fabrics are identified and, from *in situ* rock sample analyses further combined with field structural data, are interpreted on a lineament trajectory map as the trace of magmatic and tectonic structures. Our onshore/offshore study leads us to propose a two-phase kinematic model that emphasizes the role of a strike-slip duplex in an EW-trending relay zone linking the North Armorican and Pierres Noires ductile shear zones (NASZ, PNSZ). Dextral shearing occurred within a transtensional setting, synchronously with magmatic intrusions (St-Renan granite and an offshore gabbro-diorite complex) dated at 314-320 Ma by new U-Th/Pb ages. It post-dated an early regional foliation related to top-to-the-NE ductile transpresional shearing. Our study emphasizes the key role of strike-slip tectonics in the NW part of the Armorica Variscan belt.

Highlights

► Interpretation of offshore LiDAR and echosounder records. ► Structural map of Variscan ductile strain, off Leon domain, NW Brittany. ► Elaboration of a foliation trajectory map. ► Emphasis is put on regional dextral shearing. ► A new transpressional kinematic model is proposed.

Keywords : Armorican massif ; Leon metamorphic domain ; offshore structural mapping ; LiDAR records ; foliation trajectory map ; dextral ductile shearing ; U/Pb zircon/monazite dating

1. Introduction

Trajectory maps of ductile fabrics provide useful insights into the finite strain pattern and the relative chronology of deformation in pervasively deformed terrains. Drawing trajectory maps of planar ductile fabrics is generally an easy task in continuously exposed deformed terrains. This issue is much more problematical in ancient orogenic belts where basement rocks are usually highly eroded and scarcely exposed. In such unfavourable conditions, trajectory maps can be elaborated either by drawing the envelope curve of foliation trends for each discrete field measurement point, or by using geostatistical approaches. The latter method has been recently applied to specific structural domains of the Armorican Variscides (Gumiaux et al., 2004). Where ancient deformed terrains extend laterally offshore into marine areas devoid of any sedimentary cover, remote sensing imagery could be a powerful potential method for imaging submerged basement structures. Such geophysical surveys have recently been performed in the Molene archipelago, off NW Britanny (Fig. 1a), by combining LiDAR (Light airborne detecting and ranging) and multibeam swath records. The resulting composite high-resolution dataset provides an exceptional structural picture of the Variscan bedrock over a ~ 12 x 20 km area, in the western offshore extent of the Leon metamorphic domain (LMD in the text) (Fig. 1b).

It has been known for a few decades that the LMD forms an exotic terrane within the Armorican Variscides. Its overall structure is dominated by large-scale metamorphic thrust

sheets, further dissected by both sinistral (Guisseny-Porspoder; GPSZ), and more numerous dextral (North Armorican, Elorn, and Pierres Noires; NASZ, ESZ, PNSZ) ductile transcurent shear zones. In both cases, transcurent shearing is accompanied by synkinematic granitic intrusions (see Ballèvre et al., 2009, for a review). However, major uncertainties still exist with regards to the internal architecture and map trace of the entire shear zone pattern. The specific role of the ESZ and PNSZ, which separate the LMD from Paleozoic terrains of the Central Armorican domain to the south, is also debatable. These tectonic boundaries have been regarded as either dextral transform zones (Balé and Brun, 1986) or large-scale thrusts related to an oceanic suture zone (Rolet et al., 1986; Faure et al., 2005; Ballèvre et al., 2009). Possible solutions are proposed in the present paper, based on a high-resolution LiDAR/echosounder digital elevation model (DEM) that supplies, for the first time, an accurate structural map of part of the offshore Variscan basement in Brittany. Various types of planar structures, extracted from the elaborated DEM, are interpreted in terms of ductile fabrics from seafloor rock sample analyses, and correlations with strained rocks continuously exposed inland along a 10 km-long coastal section. Our offshore/onshore results, that combine a foliation trajectory map (offshore) with kinematic data (onshore), ultimately allow us to propose an improved kinematic model for part of the Variscan history of the LMD. An intricate dextral shear zone network, arranged into a regional-scale strike-slip relay zone, post-dated the earlier regional foliation associated with top-to-the-NNE shearing. The timing framework of Variscan ductile strain in the LMD is further calibrated by new U/Pb zircon dating of synkinematic intrusions.

2. Geological setting

The LMD is a 30 x 80 km granitic and metamorphic domain, NW of the Armorican massif (Fig. 1a). It is part of a mosaic of structural domains that have been juxtaposed during

the Middle/Late Carboniferous along large-scale ductile strike-slip discontinuities, including the North- and South-Armorican shear zone (Gapais and Le Corre, 1980). The strongly strained and metamorphosed rocks in the LMD differ markedly from the much less deformed terrains in the surrounding North- and Central-Armorican domains that nearly escaped Variscan shortening (Fig. 1a).

The overall structural arrangement of the LMD is generally thought to be a result of the combined effects of early large-scale thrusts, later intruded by various synkinematic granitoids during transcurrent shearing. Though not totally cylindrical, the structure of the LMD is synthetized on the 30 km-long cross-section of Fig. 1c. It shows a broad N70°E-trending upright antiform, involving a pile of thrust slices with metamorphic grades increasing northwestwards, i.e. downsection, from greenschist facies to partial-melting conditions. The upper allochthonous units in the southern flank of the antiform comprise, from top to bottom, the Brest orthogneiss, the protolith of which yielded ages of 504 ± 15 Ma (Marcoux et al., 2009), the Le Conquet amphibolite-facies micaschists and metagabbros, dated at 478 ± 4 Ma (Faure et al., 2010) and the Lesneven gneisses that pass northwards into sillimanite-rich facies with pockets of anatectic granites. The basal unit is thrust over the para-autochthonous Treglonou orthogneiss in the core of the eroded antiform. Its protolith has been dated at 385-391 Ma by U/Pb method on zircons (Marcoux et al., 2009). Published U-Th/Pb monazite ages of synthrusting metamorphism range from 340-335 Ma (Faure et al., 2010) to 315 Ma (Schulz, 2013). Relics of an earlier (439 ±12 Ma) HP eclogitic event (Paquette et al., 1987) are found locally in mafic lenses within the high-grade paragneiss exposed on the northern flank of the antiform (Cabanis and Godard, 1987).

The regional antiformal stack is cross-cut by two distinct types of ductile strike-slip shear zones that differ in age, kinematics, and types of related granitic intrusions (Figs. 1b and c). Early dextral shearing occurred to the south along (1) the PNSZ that extends as a 10-15

km-long corridor throughout a narrow band of undated (Pierres Noires) granites and part of the Brest gneisses (Chauris, 1994), and (2) the NASZ that cuts though the southern margin of the 321±5 Ma St-Renan-Kersaint synkinematic granite (U-Th/Pb monazite ages; Faure et al., 2010), in turn, secant to the south with respect to the strained Lesneven metamorphic terrains (Goré and Le Corre, 1987). Younger sinistral shearing took place further north, along the N70°E-trending PGSZ, which also acted as the root zone of the 301± 3 Ma Aber-Ildut southerly-directed granitic sheet (Le Corre et al., 1989; Marcoux et al., 2004).

Prior to our work, the offshore extent of the LMD Variscan framework was poorly documented. Published geological maps of the Molène archipelago only show a regular pattern of N70E-oriented granitic and metamorphic belts, with local structural disturbances, marked by the map curvature of the foliation in the Beniguet and Quemenes southern islands (Fig. 1b) (Chauris, 1994). Very little was known about the offshore map trace of the LMD shear zone pattern, except about those of the PNSZ which was assumed to continue westwards as a 15 km-long discontinuous range of islets (Chauris, 1994), whereas the PGSZ was correlated with the dextrally offset (15 km) North Ouessant shear zone (Andreieff et al., 1973) on both sides of the La Helle NW/SE-trending fault.

3. Offshore/onshore dataset

Between 2010 and 2011, an integrated airbone laser altimetry (LiDAR) and swath bathymetry survey, funded by IFREMER and the National Marine Park of Iroise, was carried out over a ~320 km^2 offshore area in the Molene archipelago (Fig. 2 and Table 1).

LiDAR techniques alone are commonly used in a variety of geoscience applications, including, river network analysis, structural mapping, and more generally speaking, geomorphic studies (Webster et al., 2006). However, combining aerial laser bathymetry and

echosounder records, as performed in the present work, is a much more original and complex technique that has been successfully applied in coastal and river environmental studies (Poppe et al., 2010).

3.1. LiDAR dataset

Airborne LiDAR records can provide high-resolution topographic data based on the two-way travel time of laser pulses. The resulting DEM's have proven to be an accurate tool for either mapping surficial features, such as faults (Kondo et al., 2008), or quantifying volumetric changes in beach budget contributions (Young and Ashford, 2006). The use of airborne lasers to measure bathymetry and seabed topography, however, is considerably more complex and challenging than topographic mapping because of a variety of technical and environmental problems. The readers are referred to Flood and Gutelius (1997) for a general overview of airborne laser scanning technology and principles. Water heavily absorbs the near-infrared energy of terrestrial LiDAR, making it ineffective over streams. Consequently, airborne LiDAR bathymetry (ALB) must operate in the blue-green regions of the spectrum, and traditionally these systems have been designed for maximum water penetration using a relatively high-power green laser fired at fairly low repetition rates. ALB has been successfully applied to coastal areas for bathymetric programs (Irish and Lillycrop, 1999), and to river environmental studies (Mckean et al., 2009).

For the Molene archipelago under study, ALB data were recorded in April/May 2010 over a ~170 km^2 area, i.e. 60% of the total offshore studied area, encompassing emerged lands and the shallowest offshore areas, with an elevation/depth range between +32m down to -27m (Fig. 2). The LiDAR measurements were georeferenced into the RGF93 datum used by the Global Positioning System. After correction for the influence of tides, LiDAR data were

exported into the Fledermaus software to produce ASCII grid files in 1 x1 km tiles, using a weighted moving average algorithm at 5m resolution with a weight diameter of 3.

3.2. Swath bathymetry surveys

In the present study, acoustic swath-mapping surveys were conducted in the Molene archipelago to complete the ALB dataset, using a multibeam echosounder in the deepest parts (-10 m down to -100 m), as well as an interferometric sidescan sonar in shallow water (Fig. 2).

A surface of ~54 km^2 in water depth of <20 m was investigated using the hydrographic survey boat V/O Haliotis (Ifremer), equipped with a hull-mounted GeoSwath interferometric sidescan sonar (Table 1). The GeoSwath is a fully integrated sonar tool designed for high-resolution surveys. It is based on phase measuring (interferometry) technology, which provides the advantages of a wide swath and high resolution in a compact and robust system, and is suitable for deployment in shallow waters where towed sidescan sonars have particular problems. A full description of GeoSwath system performance is given by Hiller and Hogarth (2005).

Acoustic swath-mapping surveys were also conducted over the ~97 km^2 outer part of the archipelago by the costal vessel N/O Thalia, equipped with a EM1000 hull-mounted multibeam echosounder (Fig. 2). The multibeam data acquired insonified 100% of the seafloor with at least a 20% overlap of the echosounding corridors. The Simrad EM1000 is an ultra-wide Swath sounder, suitable for surveying swaths of up to 7.5 times the water depth. Since the 90's, it has been used routinely for seafloor geological mapping of the continental shelf (Acosta et al., 2004).

Bathymetric data from 2500 acoustic profiles were first processed for corrections (filtering, sound speed velocity, navigation, tidal) with the Caraibes software (© Ifremer), in order to elaborate a DEM displaying the same vertical referential as the LiDAR dataset, and to standardize the chart datum to lowest astronomical tides.

3.3. Seafloor rock sampling

A total of 52 seafloor rock samples have been collected in selected offshore areas (Figs. 2 and 3), in order to constrain the structural interpretation of fabrics extracted from the bathymetric map of Fig. 3. Divers directly collected 15 rock samples at depths of < 20 m. The other rock samples (37) were acquired by gravity Cnexo-ville rock cores in deeper waters. Though not oriented, *in situ* rock samples provide useful informations about strain conditions. One major new insight is the recognition of a large-scale gabbro/diorite intrusive complex whose emplacement was constrained by U/Pb zircon dating.

3.4. Digital elevation model

For our study, each acquisition system results in a specific DEM with its own spatial resolution in the range 0.5 m (GeoSwath) - 5m (LiDAR) (Table 1). Data were processed using the SonarScope software (© Ifremer), by the nearest-neighbour interpolation method, and then merged to provide a unique georeferenced raster grid with a spacing of 5 x 5 m (horizontal resolution), and a maximum vertical resolution of 0.5 m.

Focused views with the highest horizontal resolution (0.5 m) were locally acquired around specific structures. The resulting gridded DEM was imported into a geographic information system (GIS) for geomorphic analyses. Improved hillshaded imagery was produced in ESRI

to enhance structural mapping. Hillshading is known to be subject to directional bias. To address this issue, two shaded relief images were first obtained by using illumination sources with two perpendicular azimuths (45° and 270°) and a constant tilt of 30°, and then superposed by transparency in order to enhance the trace of the total population of linear fabrics. The latter were then digitized manually from the bathymetric map.

4. Analysis of bathymetric and geological data

4.1. Geomorphic offshore patterns

With respect to the –10 m isobath, the Molene archipelago extends as a 10 x 20 km elongated plateau, with a NW-SE-trending elevated axial zone, outlined by six major islands (Fig. 3). It is dissected by an intricate network of NE-SW-, NW-SE-, and to a lesser extent, N-S-trending depressions, inferred to be the surficial expression of post-Variscan faults. These young brittle structures are not discussed in the present paper, with the exception of the La Helle fault used to restore the initial map-geometry of laterally offset basement structures.

4.2. *Offshore geological mapping*

The geological map of the Molene archipelago in Fig. 4 has been obtained by merging exposed geology with lithological data from seafloor rock samples (52), along with the analysis of bedrock surface roughness observed on the improved hillshaded offshore DEM (Fig. 3). Most of the metamorphic and plutonic seafloor rock samples collected offshore have onshore counterparts exposed in the islands and on the Leon mainland (Fig. 1b). Several interesting points arise from the examination of the Molene geological map. Those dealing with structural issues are discussed in the next section. Because of the intrusion of the St-

Renan and Aber-Ildut granites, the HP eclogite-bearing units involved in the northern flank of the LMD antiform do not extend laterally offshore into the studied area.

- To the south, the N70°-trending Brest gneiss unit dies out rapidly westwards as the result of its obliquity with the EW map-trace of the 1-2 km-wide mylonitic zone following the PNSZ.

- To the north, the St-Renan granite is interdigitized with migmatites of the Plouarzel complex, west of the Molene island.

- Further north, both the leucogranitic (west) and the red/porphyric (east) facies of the Aber-Ildut granite overlap the highly-strained rocks of the St-Renan-Plouarzel granitoid complex.

- The Groac'h Zu intrusive complex, identified SW of Trielen island, also includes the diorite/gabbro rocks, locally exposed, in small islets around the intrusion (Chauris and Hallegouet, 1989). New radiometric dating has been performed on collected gabbro core-rock samples.

4.3. In situ U/Pb geochronology

Available U-Th/Pb dating of monazites yielded ages of 321 ± 5 Ma for the syntectonic emplacement of the St-Renan granite along the NASZ (Faure et al., 2010), and ages of 338 ± 5 Ma (Faure et al., 2010), and 315-305 Ma (Schulz, 2013) for the amphibolite-type metamorphism recorded by the Le Conquet micaschists. In order to achieve a more complete time framework of the Variscan strain in the LMD, U-Th/Pb zircon/monazite dating has been performed, both for the offshore Groac'h Zu intrusion, and for coherency purposes, for the onshore part of the St-Renan granite.

Zircon and monazite U-Th/Pb geochronology was conducted in the Laboratoire Magmas & Volcans in Clermont-Ferrand (France) using LA-ICP-MS. The method used for dating is

similar to those developed by Paquette and Tiepolo (2007). Detailed analytical procedures and conditions used in this study can be found in Hurai et al. (2010, 2012). U, Th and Pb concentrations (available on-line as supplementary material) were calibrated relative to the certified GJ-1 zircon standard (Jackson et al. 2004), and the Moacyr monazite standard (Gasquet et al., 2010). Concordia ages and diagrams were generated using Isoplot/Ex v. 2.49 (Ludwig 2001). The zircon and monazite analytical results were projected on $^{207}Pb/^{206}Pb$ *versus* $^{238}U/^{206}Pb$ diagrams (Tera and Wasserburg, 1972) and $^{206}Pb/^{238}U$ *versus* $^{208}Pb/^{232}Th$ diagrams, respectively.

The dated sample from the Groac'h Zu intrusion is a highly altered but unstrained gabbro-diorite (cv10 in Fig. 3). It is composed of large plagioclase and amphibole grains, as well as oxides and apatite. Biotites or pyroxenes are pseudomorphosed into chlorite. Small, rare quartz grains are also present. The zircon crystals are translucent, yellow, and subhedral, but appear partly broken. This hypidiomorphic shape of the zircon grains has already been observed in Variscan gabbros (Gebauer, 1990; Paquette et al., 1995), and is merely due to the morphology of the free areas between the surrounding minerals, when zircon crystallizes as a late phase in the magma.

Two fresh samples from the St-Renan granite have been collected in a quarry near St Renan (Location in Fig. 1). Sample 13DB10 is a fine-grained granite with quartz, microcline, feldspars, and small grains of biotite and muscovite. Sample 13DB11 is more porphyric. It contains less quartz, a greater amount of biotite, and some large feldspars. Neither magmatic nor tectonic fabrics are present in these samples. Zircon crystals are translucent, colourless to light brown, euhedral, and short prismatic. Monazites are yellow to brown and also euhedral. Morphologies of both mineral types are very similar and may be confused.

A set of thirty-four 33 µm-wide spots were analyzed by laser ablation coupled to ICP-MS on cv10 single zircon crystals (Fig. 5d). All the analyses are concordant, and yield an age of

317.9 ± 2.0 Ma (Fig. 5) which is the crystallization age of the zircons during the emplacement of the gabbro-diorite. U content generally ranges between 100 to 300 ppm and Pb content is close to 10 ppm. The Th/U ratios of 0.3 are characteristic of magmatic zircons.

Twenty-seven 20 µm-wide laser spots were performed on the 13DB-10 and on eleven zircon crystals from the granite. Ten spots measured in zircon cores and one whole crystal display a large range of ages, mostly from 380-410 Ma (Fig. 5b) up to 980 Ma and 1.8 Ga (Fig. 5a and supplementary material). These inherited ages are related to the crust recycling during the granite petrogenesis. The remaining seventeen spots measured on whole-grains and outer rims are concordant in the U/Pb diagram, and yield an age of 316.0 ± 2.0 Ma (Fig. 5b). A set of twenty-seven 10 µm-wide laser spots was performed on the monazite crystals from the same St-Renan granitic samples. Twenty-one analyses, concordant in the U/Th/Pb diagram, define an age of 316.7 ± 1.5 Ma (Fig. 5c), i.e. similar to that obtained on the zircons, and precise the crystallisation age of the rock. The six remaining analyses are scattering between 330 and 360 Ma (Fig. 5c) and, similar to the zircons, recorded previous geological events of the protoliths.

These new results undoubtedly demonstrate that both gabbro and granite samples are contemporaneous at 316-318 Ma. Our dating of the St-Renan granite is compatible within error limits with the 321 ± 5 Ma age on monazites previously obtained by the EMPA technique (Faure et al., 2010).

4.4. *Magmatic/tectonic ductile 2D-pattern*

Lineaments extracted from the high-resolution bathymetric map of Fig. 3 are assumed to represent the trace of regional-scale structures in the basement seafloor. Five distinct types of linear fabrics (labeled ‘a to e’) are identified from their specific physical attributes (length, spacing, spatial distribution, sinuosity, and cross-cutting relationships). Their structural interpretation is based on evidence from seafloor rock samples, structural map features, lateral

onshore correlations, and kinematic criteria supplied by the St-Mathieu-Corsen reference coastal section (next paragraph). Most of the offshore area under study is dissected by a dense network of closely-spaced and short lineaments, confidently regarded as the map-trace of Variscan penetrative ductile structures (Fig. 4). These key features, extensively discussed in the paper, are cut by a discrete network of fault-like structures, probably late-to post-Variscan in age, and are not addressed here.

The first type of linear lineaments (fabric 'a') is marked by a submeridian network of fault-like discontinuities, spatially confined within granitic intrusions. To the north, in the Alber-Idult granite (Fig. 3), they delineate a pattern of <100 m-wide elongated substratum blocks and intervening flat-bottomed sedimentary depressions (Fig. 6a1). They correlate onshore, in the Lampaul-Plouarzel area, with vertical cooling joints that likely formed at a late stage of granite emplacement (Figs. 3and 6a2).

More closely-spaced lineaments extend with a N120°E orientation NE of the Aber-Ildut granite (fabric 'b' on Fig. 6b1). Their onshore continuation to the SE corresponds to a composite planar structure, in a vertical position, involving a magmatic flow pattern overprinted by a later network of (~1m-spaced) tectonic joints (Fig. 6b2). These late magmatic features are not discussed here. Conversely, emphasis is placed on more widely-distributed lineaments, occurring preferentially in the southern half of the offshore studied area, and among them three types of fabrics are recognized.

- Fabric 'c' is marked by a closely-spaced network of lineaments, extending with a dominant N70°E orientation, over a length of > 1 km (Figs. 4 and 6c1). It represents the regional foliation, as indicated by the *in situ* micaschist rock sample cv8, and by the micro-structure of rock sample cv29 that shows a typical gneissic fabric (Lesneven series) expressed by bands of elongated quartz-FK-plagioclase and biotite-muscovite assemblages (Fig. 3). At a

larger scale, fabric ‘c’ lineaments pass laterally onshore into the foliated Le Conquet micaschists (Fig. 6c2).

- Fabric ‘d’ corresponds to sigmoidal lineaments, spatially restricted within narrow (1-2 km-wide) and elongated (>10 km-long) corridors that typically resemble ductile shear zones (Ramsay and Graham, 1970) (Figs. 4 and 6d). The obliquity of the internal C/S-type patterns indicates dextral or sinistral shearing (Figs. 6d1a, d1b). C/S-type fabrics are also observed as micro-scale structures in offshore *in-situ* samples showing thin bands of asymmetrical quartz and K-feldspar porphyroclasts (S), further dissected by oblique shear planes (C) (samples cv2, Pierres Noires granite; cv24, Plouarzel migmatite; cv29, Lesneven gneiss; Fig. 3). Shear criteria are also documented onshore, as dextral C/S ductile fabrics in high-strained St-Renan granitic facies involved in the NASZ (Figs. 3 and 6d2b), or as sinistral C/S fabrics in Lesneven orthogneisses (Figs. 3 and 6d2a).

- Fabric ‘e’ is chiefly expressed to the southwest by sinuous and more widely-spaced lineaments, drawing a 5 km-wide fold-like structure, parallel to the metamorphic host-rock foliation, in the so-called Graoc'h Zu intrusive complex (Figs. 4 and 6e1). The thin section of the corresponding granite seafloor rock sample (p11) shows the preferred linear orientation of most porphyroclasts (quartz, FK, plagioclase, micas), with no evidence of tectonic strain (Fig. 3).

4.5. Onshore kinematic dataset along the St-Mathieu-Corsen coastal section

Structural analysis of the metamorphic units continuously exposed along the St-Mathieu-Corsen coastal section (Fig. 7) has been performed in order to further constrain offshore/onshore structural correlations, and also to provide accurate kinematic criteria. The exposed metamorphic rocks, of Paleozoic age (Cabanis et al., 1979), form a S/SE-dipping monoclinal structure, intruded to the north by unstrained facies of the St-Renan granitic

massif (Fig. 7). These rocks have been deformed under amphibolite facies conditions that increase northwards, i.e. towards the structurally lower parts of the crustal pile, from the gneiss of Brest, the Le Conquet micaschists, down to the gneiss of Lesneven (the reader may refer to Jones, 1993, 1994; Schulz, 2013, for a detailed description of the metamorphic history). Anomalous superposition of either metamorphic units (inverted grades, high grade-over lower grade-rocks), or structural units (abrupt strain gradients), which should have provided arguments for major tectonic contacts as postulated by Faure et al. (2010), are missing along the overall transect under study (Schulz et al., 2007). The presence of an oceanic suture zone, outlined by the metagabbro-amphibolite lenses within the Le Conquet micaschists (Faure et al., 2005; 2008), is also unlikely since the ophiolitic nature of the metabasites is yet to be demonstrated (Ballèvre et al., 2009; Schulz, 2013).

Evidence for superimposed structures exists more frequently along the southern part of the section. An analysis of porphyroblast inclusions has been used to argue for a polyphased ductile strain history (5 distinct phases reported by Jones, 1994). However, most exposed strained rocks display a single foliation (S), generally associated with a shear plane (C) in porphyric/coarse-grained facies. The map-trace of the regional foliation in Fig. 7 strictly follows the offshore lineament pattern labeled ‘c’ in Fig. 6. The main goal of our structural field study is only to discriminate various styles of structures and strain within spatially distributed structural domains that might correlate laterally with the ductile fabrics identified on the offshore DEM of Fig. 3. Defining the precise strain/stress history of the LMD metamorphic rocks is beyond the scope of this paper.

Three distinct structural domains, with specific ductile deformation styles, are distinguished on the 10 km-long transect (Figs. 7 and 8). Two of them roughly correspond to those previously described, involving top-to-the-NNE thrust-related shear (Faure et al., 2010), and dextral transcurrent shear (Balé and Brun, 1986; Goré and Le Corre, 1987). Additional

kinematic data are supplied by our detailed structural study that further enable us to identify a third type of structural domain, evoked by Jones (1994) as being dominated by transtensional shear in a spatially restricted zone.

The most relevant deformational features of each structural domain are briefly described, below.

- *Domain (a) : Dominant top-to-the-NE thrust-related shear*

Domain (a) is here referred to as a 5 km-wide zone that nearly coincides with the Lesneven gneissic unit, exposed on the northernmost part of the transect (Figs. 7 and 8b). The dominant outcrop-scale structure is a foliation plane (S), striking northeasterly, and dipping steeply to the southeast. An anomalous zone exists in the Brenterc'h area, where a pronounced shallowing of the foliation dip (down to ~25°) is accompanied by the counter-clockwise rotation of its trend toward the north (Fig. 7). That map-scale deflection evokes a post-foliation fold compatible with sinistral shearing. A stretching lineation (L) locally lies within S as elongated quartz-feldspar assemblages. It displays a wide range of steeply plunging attitudes, generally >45°, and consistently toward the SW (Fig. 8a). On the XZ planes, orthogonal to S and parallel to L, S is locally associated with a shear plane (C) (Fig. 8b). The resulting composite S/C planar fabric systematically shows a top-to-the-NE sense of shear. If assuming, to a first approximation, that L indicates the transport or shear direction of deformation, it follows that the NE-directed displacement is oblique, and combines a prominent top-to-the-N reverse component (Fig. 8c1), in addition to sinistral ductile shearing (Fig. 8b). A similar sense of (post-foliation) shear is deduced from the above-mentioned map-scale fold.

- *Domain (b) : dextral ductile shearing*

Two discrete zones typically show structural features of pure strike-slip ductile shear at the two extremities of the transect (Fig. 8b). To the north, tourmaline-bearing facies of the St-Renan granite are highly deformed along a 1.5 km-wide zone, occurring 1-2 km north of its magmatic contact with the foliated Lesneven gneiss (see above). That is the coastal section of the NASZ in which the main fabric corresponds to subvertical anastomosing foliation (S) and shear (C) planes, striking E-W on average (Fig. 7). On the S-surface, a well-developed stretching lineation is outlined by elongated K-feldspars in a sub-horizontal position (e.g. Goré and Le Corre, 1987, for details). When observed in XZ sections, the S/C fabric indicates a rotational deformation, as well as a dextral sense of shear (Fig. 8b).

To the south, orthogneisses and a subordinate metasedimentary sequence of quartzitic layers and metapelites of the Brest unit both occur from a vertical to a southerly-dipping position within a ~1 km-wide zone extending from St Mathieu to Penzer (Figs. 7 and 8b). Within the so-called PNSZ, the orthogneisses are penetratively deformed by a composite S/C planar fabric, in a vertical position, striking N80°E (Figs. 7 and 8b). The preferred elongation of quartz-feldspar assemblages on the S-planes outlines a sub-horizontal to shallowly-plunging stretching lineation (Fig. 8c6). Sigmoid-shaped K-feldspar and quartz phenocrysts observed in XZ sections indicate dextral shear (Fig. 8c5). A similar sense of shear is also recorded by dextrally folded mylonitic bands. Ductile dextral shearing is expressed in another way in the vertical quartzite-metapelite sequences by asymmetrical and steeply-plunging isoclinal folds displaying an axial plane parallel to the N80°-oriented schistosity of the metapelites. Further north, criteria for dextral shearing still exist, but in moderately-inclined gneisses (Brest unit) (Figs. 8a, b).

- Domain (c) : polyphase and extensional ductile strain

The third structural domain involves most of the Le Conquet micaschists unit exposed from Penzer to Portez beach (Fig. 8b). With respect to the two other structural domains, this 2.5 km-long intermediate domain is demarcated by a more shallow (southerly) dip of the foliation, generally <45°S, and a conspicuous stretching lineation (L), with variable plunging azimuths (Fig. 8a). L is defined by various markers, including quartz pressure-shadows on garnet porphyroblasts, and corrugated and/or boudinaged quartz layers (Fig. 8c4). In many places, the strong development of the lineation results in a S-L-type tectonic fabric in the Le Conquet micaschists (Porz Liogan in Fig. 8b). The diagram of Fig. 8a shows its wide range of plunge within S, but with an asymmetrical distribution to the SW. The prominent southwesterly-plunging lineation, generally outlined by either sigmoidal K-feldspars in gneissic facies, or by tails and pressure-shadows on rotated garnets in micaschists (Fig. 8c3), is systematically associated with a component of dextral shear. That resulted in a bulk SW-directed trans-tensional displacement on the S surfaces (Fig. 8b), already evoked by Jones (1994). In the northern part of domain (c), from Porz Liogan to Portez (Fig. 7), SW-directed extensional shearing coexists with top-to-the-N reverse shear which is recorded by rotated inclusions (S1) in garnets (Faure et al., 2010).

Since the two opposite shear strains both display a nearly parallel NE-SW transport lineation, evidence for superimposed patterns are not easily documented within domain (c). Nevertheless, a relative timing framework can be reasonably deduced from the following evidence. More convincing structures are supplied by the interference pattern in Fig. 8c2. It shows an early foliation, affected by N-verging asymmetrical folds, both being dissected by a dense network of top-to-the-S extensional shear bands. Porphyroblast/foliation relationships in garnet-bearing micaschists also provide additional supportive evidence (Fig. 8c3). The early foliation, preserved as inclusions in rotated garnets, is tentatively regarded as remnants

of top-NE reverse shear-related structures (Faure et al., 2010), later overprinted by the regional foliation and its spatially associated SW-directed extensional shear planes.

4.6. Regional ductile strain framework

The structural sketch map in Fig. 9 combines both the offshore lineament trajectory map of Fig. 4, obtained by extrapolating the trace of various ductile fabrics, and structural and kinematic data from the SW Leon coastal section. Three major types of magmatic/tectonic ductile structures are clearly identified : the internal fabric of the Groac'h Zu intrusion, the regional foliation, and a number of discrete shear zones. Their mutual interference patterns, in addition to newly acquired radiometric ages of intrusions, supply accurate temporal constraints for the kinematic model proposed in the last paragraph.

The more widely distributed fabric is the regional foliation which coincides accordingly with the offshore continuation of the LMD metamorphic terrains to the SE (Fig. 9). The offshore foliation pattern is dissected by six shear zones, with C/S internal fabrics that indicate a dextral sense of shear for five of them, the so-called Fromveur, North Molene, Groach Zu, Beniguet, and Pierres Noires shear zones (FSZ, NMSZ, GZSZ, BSZ and PNSZ, respectively). The only sinistral shear zone, i.e. the South Molène shear zone (SMSZ), is cut to the east, and post-dated by the St-Renan granite (Fig. 4). The SMSZ is thus assumed to be linked to top-to-the-NE shear strain that also comprises a sinistral component onshore, whilst being post-dated by the St-Renan granite.

Concerning the prominent dextral shear zone pattern, offshore/onshore correlations can be readily constructed about the EW-trending PNSZ that extends continuously throughout the coastline (Figs. 4 and 9). On the contrary, the offshore extent of the NASZ is more problematic, being erased by Quaternary deposits, and further dextrally offset by the La Helle fault (Fig. 4). Among the two possible candidates, i.e. the N70°E-oriented FSZ and NMSZ,

the latter is the more appropriate structure, given (1) its ~ 4 km apparent dextral offset with regards to the onshore NASZ, i.e. similar to the offset of the reference Aber Ildut granite on both sides of the La Helle fault (Fig. 4), and (2) the nearly similar 10 km map-distance between the NMSZ and NOSZ (offshore), and between the NASZ and PGSZ (onshore), keeping in mind that the NOSZ is the western counterpart of the GPSZ (Fig. 1b).

Further south, complex interactions exist between the GZSZ and BSZ dextral shear zones, the regional foliation, and the Groac'h Zu intrusion (Figs. 9 and 10). The BSZ appears to merge southwards onto the EW-oriented PNSZ, whereas to the NE it transects the EW trace of the regional foliation (Figs. 10b, e). To the north, the GZSZ forms the southern tectonic boundary of the Groac'h Zu intrusive complex, cutting through its concentric internal fabric that however tends to merge into the map-trace of the shear zone (Fig. 10b). Given the unstrained character of the cv10 (gabbro) and p11 (granite) *in situ* seafloor rock samples (see above), the internal fabric of the Groac'h Zu intrusive complex is assumed to be a magmatic feature (compositional layering or magmatic flow).

Between the two shear zones, the foliation draws large-scale asymmetrical folds, kinematically consistent with dextral shearing (Fig. 10d). Beyond the NE tip zone of the two shear zones, the foliation is severely disrupted and folded along a submeridian network of sinistral faults (Fig. 10c). To the NW, the foliation shows a map-scale deflection around the northern elliptic trace of the intrusion boundary.

5. Discussion and conclusions

5.1. Tectonic event chronology

The two successive episodes of ductile strain previously identified on the southern flank of the regional-scale LMD antiform (Balé and Brun, 1986; Rolet et al., 1986) are

confirmed in the present work. However, our onshore/offshore structural approach allows us to accurately detail both the kinematics (onshore) and spatial extent (offshore) of their respective deformations.

A first episode of top-to-the-NE transpressional ductile shear, associated with a sinistral shear component, resulted in the development of the N70-80°E regional foliation. To a first approximation, this early strain pattern is kinematically compatible with a maximal principal stress axis in the NE quadrant. The N70°E sinistral SMSZ identified in the offshore lineament trajectory map is assumed to be a map-scale expression of the sinistral shear component documented onshore. Both the foliation (onshore) and the SMSZ are cut and thus post-dated by the 316 ± 2 Ma-old St-Renan granite.

Evidence for a second episode of transtensional ductile tectonics is found, both onshore, in spatially restricted areas, and offshore in five dextral shear zones. Onshore, the deformation is partitioned into discrete dextral strike-slip shear zones, and top-to-the-SW transtensional shear zones. In terms of regional stress conditions, the dextral transtensional strain pattern likely developed in response to the counter-clockwise rotation of the maximal principal stress axis in the NW quadrant. During this episode, magmatic intrusions took place in close connection with dextral shear zones. The synchroneity of the St-Renan granite (dated here at ~316 Ma) and the NASZ has long been advocated onshore (Goré and Le Corre, 1987). Syntectonic emplacement of the coeval (~318 Ma) Groac'h Zu intrusion along the dextral GZSZ is also supported here by the fact that its internal magmatic fabric tends to merge into the southern sheared boundary of the intrusion. Additional supportive evidence is observed immediately east of the intrusion, where the foliated structure of the country-rocks is highly disturbed by a submeridian network of sinistral faults. By analogy with results of experimental modeling of a rigid rotated body within a viscous matrix during simple shear

(Van den Driessche and Brun, 1992), these structures are assigned to the clockwise rotation of the pluton at a cooling stage, during progressive dextral shearing.

Along with our onshore structural data (Figs. 7 and 8), the mutual relationships between the Groac'h Zu intrusion, the shear zones, and the regional foliation supply additional constraints for the temporal development of the two successive strain events. Indeed, the emplacement of the Groac'h Zu intrusion by progressive ballooning in previously strained terrains (first shear episode) might have caused, concomitantly with dextral ductile shearing, later deformation (folds) in the foliated country-rocks around the southern intrusion boundary (Fig. 10).

The third shearing event that occurred at ~300 Ma further north along the N70°E sinistral PGSZ (Le Corre et al., 1989) has no structural expression in our study area. Both its kinematics and trend likely resulted from the back-rotation of the stress axes.

With regards to the numerous published structural, metamorphic, and radiometric data (e.g, Paquette et al., 1987; Le Corre et al., 1989; Jones, 1994; Godard and Mabit, 1998; Schulz et al., 2007; Faure et al., 2010; Schulz, 2013), we find it difficult to correlate the tectonic events argued here with the metamorphic episodes reported by previous authors. According to Faure et al. (2010), an early HP metamorphic event and a second MP-MT event are coeval with top-to-the-N thrusting at <340 Ma, whereas a third MP-HT event operated synchronously with younger dextral shearing at 335-327 Ma. The two metamorphic episodes of Schulz et al. (2007) and Schulz (2013) consist of a first HP event related to crustal thrusting at 360-340Ma, and a second MP-MT to -HT event at 340-300 Ma within a dextral transtensional setting.

Consequently, the N-verging thrust episode of Faure et al. (2010) roughly correlates with our first top-to-the-NE shear event, and its associated age, around 340 Ma, is in accordance with our timing (older than 320 Ma). The second top-to-the-SW extensional shear

event emphasized here has not been observed by these authors. On the other hand, transtensional tectonics is suggested by Schulz et al. (2007) and Schulz (2013), but his corresponding time-range (340-300 Ma) is much larger than the robust U/Pb ages acquired in the present study.

5.2. Dextral shear zone pattern

One of the new insights from our structural work is the identification, in the offshore extent of the LMD, of a much more intricate dextral shear zone pattern than those previously reported from onshore data that includes only part of the NASZ and PNSZ (Fig. 1b). The overall map arrangement of the offshore/onshore dextral shear zone pattern, once completed to the SE by the Elorn Shear Zone (ESZ), shows a linked system composed of two major EW-striking segments, i.e. the NASZ and PNSZ, that connect *via* a 10 x 80 km overlapping zone (Fig. 11). This relay zone comprises an array of second-order right-lateral shear zones, striking N70°E, i.e. the ESZ, BSZ, GSSZ and FSZ. According to the terminology of Woodcock and Fisher (1986), the overall system mimics a strike-slip duplex compatible with a relay zone in an EW-trending dextral system. The resulting stretching direction should be NE-SW, i.e. nearly parallel to the mean mineral lineation related to our transtensional tectonic event onshore. The 80 km-long relay zone identified here is thus a new major structural feature in the dextral transcurrent network that dissected the Armorican Variscides during the Late Carboniferous (Fig. 11). One implication of our findings is that it rules out the 'transform' model of Balé and Brun (1986) that implied the extent of the ESZ beyond the PNSZ, as far south as the South Armorican domain.

The structural sketch in Fig. 11 also emphasizes the spatial association of the ~ coeval St-Renan and Groac'h Zu intrusions with the NASZ and GZSZ/PNSZ, respectively. In detail, we also observe the asymmetrical drop-shaped map-trace of the various magmatic intrusions

along the NASZ and PNSZ, with their long axis oblique to the shear zones (Fig. 11). Similar geometries have long been considered as criteria for the synchronism of granitisation and dextral shearing along, for example, the eastern course of the NASZ (Guillet et al., 1985), or the SASZ (Hanmer and Vigneresse, 1980). Furthermore, the close spatial association of the intrusions and dextral shear zones suggests strong interactions between pluton-induced thermal weakening of the crust and the location of discrete crustal-scale shearing.

One other important issue concerns the structural significance of the transtensional tectonic regime documented onshore. According to Jones (1994) and Schultz (2007), it might have accompanied the progressive exhumation of the entire LMD metamorphic terrains during a HT event. However, given the restricted spatial distribution of these structures, further fieldwork is really needed to assess whether the transtensional tectonic regime strictly resulted from either the relay zone kinematics, or a crustal-sale exhumation process during late orogenic collapse. From this point of view, the origin of the Leon antiform as a compressive structure (Rolet et al., 1986) can be also questioned, and possibly substituted by a 'metamorphic core complex' hypothesis. In this way, fruitful comparisons could be attempted with the nearly contemporaneous extensional systems that also characterized the South Armorican Variscan belt (Gapais et al., 1993; Cagnard et al., 2004; Turrillot et al., 2009; 2011).

Acknowledgments

The Parc Naturel Marin d'Iroise (Philippe Le Nilliot) and the SHOM are acknowledged for permitting publication of the LiDAR and echosounder offshore data. Petrological correlations with onshore granites has greatly benefitted from the expertise of Martial Caroff (Brest university). Many thanks to Jean-Pierre Oldra for making the thin sections. This work benefited from a State Grant (A.A.) from the French Agence Nationale de

la Recherche in the Program ANR-10-LABX-19-01, Labex Mer, and from Swiss National Science Foundation (SNSF) grant no. PA00P2-145309 (DB). We thank Romain Augier and Denis Gapais who helped improve this manuscript.

References

J. Acosta, M. Canals, A. Carbó, A. Muñoz, R. Urgeles, A. Muñoz-Martín, E. Uchupi. 2004. Sea floor morphology and Plio-Quaternary sedimentary cover of the Mallorca Channel, Balearic Islands, Western Mediterranean. Mar. Geol., 206, 165–179.

P. Andreieff, J.P. Lefort, A. Marec, C. Onciardini. 1973. Les terrains antécambriens et paléozoïques au large du Léon et leur relation avec la couverture secondaire et tertiaire de la Manche. Bull. Soc. Géol. Minéral. Bretagne, V (1), 13-20

P. Balé, J.P. Brun. 1986. Les complexes métamorphiques du Léon (NW Brittany) : un segment du domaine éohercynien sud-armoricain translaté au Dévonien. Bull. Soc. Géol. Fr., 8, (2), 471-477.

M. Ballèvre, V. Bosse, C. Ducassou, P. Pitra. 2009. Paleozoic history of the Armorican Massif. Models for the tectonic evolution of the suture zones. C. R. Géosciences, 341, 174-201.

B. Cabanis, J.-J. Peucat, J. Michot, S. Deutsch. 1979. Remise en cause de l'existence d'un socle orthogneissique antécambrien dans le pays de Léon : étude géochronologique par les méthodes Rb/Sr et U/Pb des othogneiss de Tréglonou et Plounevez-Lochrist. Bull. BRGM, 14, 357-364.

B. Cabanis, G. Godard. 1987. Les éclogites du Pays de Leon (NO du Massif armoricain) : étude petrologique et géochimique ; implications géodynamiques. Bull. Soc. Géol. Fr., 8, (3), 1133-1142.

F. Cagnard, D. Gapais, J.-P. Brun, C. Gumiaux, J. Van Den Driessche. 2004. Late pervasive crustal-scale extension in the south Armorican Hercynian belt (Vendée, France). J. Struct. Geol., 26, 435–449, doi:10.1016/j.jsg.2003.08.006.

J.-P. Callot, L. Geoffroy, J.-P. Brun, 2002. Development of volcanic margins: three dimensional laboratory models. Tectonics, 21. doi:10.1029/2001TC901019.

L. Chauris. 1994. Notice explicative de la feuille Plouarzel/île d'Ouessant à 1/50000, BRGM, Service Géologique National, Orléans.

L. Chauris, B. Hallégouët. 1989. Feuille Le Conquet à 1/50000, BRGM, Service Géologique National, Orléans.

J.R. Darboux, B. Le Gall. 1986. Les Montagnes Noires: cisaillement bordier méridional du basin carbonifère de Chateaulin (Massif armoricain, France). Caractéristiques structurales et métamorphiques. Geodin. Acta, 2, 121-133.

M. Faure, C. E. Bé Mézème, M. Duguet, C. Cartier, J.-Y. Talbot. 2005. Paleozoic tectonic evolution of Medio-Europa from the example of the French Massif Central and Massif Armoricain. In: The Southern Variscan belt, (ed) R. Carosi, J. of Virtual Explo., 19, ISSN 1441-8142, pap. 5.

M. Faure, E. Bé Mézème, A. Cocherie, P. Rossi, A. Chemenda, D. Boutelier. 2008. Devonian geodynamic evolution of the Variscan Belt, insights from the French Massif Central and Massif Armoricain. Tectonics, 27, 19, doi:10.1029/2007 TC002115.

M. Faure, C. Sommers, J. Melleton, A. Cocherie, O. Lautout. 2010. The Léon domain (French Massif armoricain): a westward extension of the Mid-German Crystalline Rise? Structural and geochronological insights. Intern. J. Earth Sc., 99, 65-81.

M. Flood, B. Gutelius. 1997. Commercial implications of topographic terrain mapping using scanning airborne laser radar. Remote Sensing, 63, 363-366.

D. Gapais, C. Le Corre. 1980. Is the Hercynian belt of Brittany a major shear zone ? Nature, 288, 574-576.

D. Gapais, J.-L. Lagarde, C. Le Corre, C. Audren, P. Jégouzo, A. Casas Sainz, J. Van den Driessche. 1993. La zone de cisaillement de Quiberon : témoin d'extension de la chaîne varisque en Bretagne méridionale au Carbonifère. C. R. Acad. Sci. Paris, III, 316, 1123-1129.

D. Gasquet, J.-M. Bertrand, J.-L. Paquette, J. Lehmann, G. Ratzov, R. De Ascenção Guedes, M. Tiepolo, A.-M. Boullier, S. Scaillet, S. Nomade. 2010. Miocene to Messinian deformation and hydrothermalism in the Lauzière Massif (French Western Alps): New U-Th-Pb and Argon ages. Bull. Soc. Géol. Fr., 181, 227-241.

D. Gebauer. 1990. Isotopic systems-Geochronology of eclogites. In : Eclogite Facies Rocks, ed. D.A. Carswell, 6, 141-158.

G. Godard, J-L. Mabit. 1998. Peraluminous sapphirine formed during retrogression of a kyanite-bearing eclogite from Pays de Léon, Armorican Massif, France. Lithos. 43, 15-29

B. Goré, C. Le Corre. 1987. Cinématique hercynienne du cisaillement nord-armoricain à la bordure du granite syntectonique de Saint-Renan. Bull. Soc. Géol. Fr. 8, 3, 811-819

P. Guillet, J.-L. Bouchez, Vigneresse J.-L. 1985. Le complexe granitique de Plouaret (Bretagne) : mise en évidence structurale et gravimétrique de diapirs emboîtés. Bull. Soc. Géol., Fr., 8, 4, 503-513.

C. Gumiaux, D. Gapais, J.P. Brun, J. Chantraine, G. Ruffet. 2004. Tectonic history of the Hercynian Armorican shear belt (Brittany, France). Geodin. Acta, 17, 289-307.

S. Hanmer, J.-L. Vigneresse. 1982. Mise en place de diapirs syntectoniques dans la chaîne hercynienne : exemple des massifs leucogranitiques de Locronan et de Pontivy (Bretagne Centrale). Bull. Soc. Géol., Fr., 7, 2, 193-202.

T.M. Hiller, P. Hogarth. 2005. The Use of Phase Measuring (Interferometric) Sonars: Choosing Appropriate Data Processing Methodologies. Intern. Hydrograp. Rev., 6, 1.

V. Hurai, J.-L. Paquette, M. Huraiová, P. Konečný. 2010. Age of deep crustal magmatic chambers in the intra-Carpathian back-arc basin inferred from LA-ICPMS U-Th/Pb dating of zircon and monazite from igneous xenoliths in alkali basalts. J. Volc. Geo. Res., 19, 275-287.

V. Hurai, J.-L. Paquette, M. Huraiová, M. Sabol. 2012. U-Pb geochronology of zircons from fossiliferous sediments 1 of the Hajnáčka I maar (Slovakia) – type locality of the MN16a biostratigraphic subzone. Geol. Mag., 149, 989-1000.

J.L. Irish, W.J. Lillycrop. 1999. Scanning laser mapping of the coastal zone: the SHOALS system. ISPRS J. of Photogram. & Remote Sens., 54, 123-129.

S.E. Jackson, N.J. Pearson, W.L. Griffin, E.A. Belousova. 2004. The application of laser ablation-inductively coupled plasma-mass spectrometry to in situ U/Pb zircon geochronology. Chem. Geol., 211, 47-69.

K.A. Jones. 1993. Phase relations in Al_2SiO_5 polymorphs; Le Conquet region, north-western Brittany, France. Proc. Ussher Soc., 8, 138-144.

K.A. Jones. 1994. Progressive metamorphism in a crustal-scale shear zone : An example from the Leon region, NW Brittany, France. J. of Metam. Geol., 12, 69-88.

H. Kondo, S. Toda, K. Okumura, K. Takada, T. Chiba. 2008. A fault scarp in an urban area identified by LiDAR survey: A Case study on the Itoigawa–Shizuoka Tectonic Line, central Japan. Geomorphology, 101, 4, 731–739.

C. Le Corre, P. Balé, Y. Georget. 1989. Le Léon : un domaine exotique et géophysique au NO de la chaîne varisque armoricaine (France). Geodyn. Acta, 3 (2), 57-71.

J.-P. Lefort. 1977. Les prolongements submergés du massif armoricain : étude de géologie et de géophysique marine. Mém. Soc. Géol. Fr., 130, 1-68.

K.R. Ludwig. 2001. User's manual for Isoplot/Ex Version 2.49, a geochronological toolkit for Microsoft Excel. Berkeley Geochronological Center, Spec Pub., 1a, Berkeley, USA, 55 p.

E. Marcoux, L. Chauris, B. Hallegouet, P. Guennoc, D. Thieblemont. 2004. Notice explicative de la feuille Plouguerneau à 1/50000, BRGM, Service Géologique National, Orléans, 144 p.

E. Marcoux, A Cocherie, G. Ruffet, J.R. Darboux, C. Guerrot. 2009. Géochronologie revisée du dôme du Léon. Géologie de la France, 1, 19-40.

J. McKean, D. Nagel, D. Tonina, P. Bailey, C.W. Wright, C. Bohn, A. Nayegandhi. 2009. Remote sensing of channels and riparian zones with a narrow-beam aquatic-terrestrial LiDAR. Remote Sensing, 1, 1065-1096.

J.L. Paquette, P. Balé, M. Ballevre, Y. Georget. 1987. Géochronologie et géochimie des éclogites du Léon: nouvelles contraintes sur l'évolution géodynamique du Nord-Ouest du Massif armoricain. Bull. of Mineral., 110, 683-696.

J.-L. Paquette, M. Tiepolo. 2007. High resolution (5 µm) U–Th/Pb isotopes dating of monazite with excimer laser ablation (ELA)-ICPMS. Chem. Geol., 240, 222–237.

J.-L. Paquette, P. Monchoux, M. Couturier. 1995. Geochemical and isotopic study of a norite-eclogite transition in the European Variscan belt: implications for U/Pb zircon systematics in metabasic rocks. Geochim. Cosmochim. Acta, 59, 1611-1622.

L.J. Poppe, W.W. Danforth, K.Y. McMullen, C.E. Parker, P.G. Lewit, E.F. Doran. 2010. Integrated multibeam and LiDAR bathymetry data offshore of New London and Niantic, Connecticut: U.S. Geol. Surv., 1231, http://pubs.usgs.gov/of/2009/1231.

J.G. Ramsay, R.H. Graham. 1970. Strain variations in shear belts. Can. J. of Earth Sci., 7, 786-813.

J. Rolet, B. Le Gall, J.R. Darboux, P. Thonon, M. Gravelle. 1986. L'évolution géodynamique dévono-carbonifère de l'extrémité occidentale de la chaîne hercynienne d'Europe sur le transect Armorique-Cornwall. Bull. Soc. Géol. Fr., 8, (2), 43-54.

B. Schulz. 2013. Monazite EMP-Th-U/Pb age pattern in Variscan metamorphic units in the Armorican Massif (Brittany, France). German J. Geosci. 164, 313-335.

B. Schulz, E. Krenn, F. Finger, H. Bratz, R. Klemd. 2007. Cadomian and Variscan metamorphic events in the Leon domain (Armorican massif, France) : P-T data and EMP monazite dating. In : The evolution of the Rheic ocean from Avalonian-Cadomian active margin to Alleghenian-Variscan collision, eds. U. Linneman, R. Nance, P. Kraft. Geol. Soc. Am., Sp. Pap., 423, 267-285.

F. Tera, G.J. Wasserburg. 1972. U-Th-Pb systematics in three Apollo 14 basalts and the problem of initial Pb in lunar rocks. Earth Planet Sci. Lett. 14, 281-304.

P. Turrillot, R. Augier, M. Faure. 2009. The top-to-the-southeast Sarzeau shear zone and its place in the late-orogenic extensional tectonics of southern Armorica. Bull. Soc. Géol. Fr., 247-261.

P. Turrillot, R. Augier, P. Monié, M. Faure. 2011. Late orogenic exhumation of the Variscan high-grade units (South Armorican Domain, western France), combined structural and 40Ar/39Ar constraints. Tectonics, 30, doi:10.1029/2010TC002788.

J. Van den Driessche, J.-P. Brun. 1992. Tectonic evolution of the Montagne Noire (French Massif Central) : a model of extensional gneiss dome. Geodin. Acta, 5, 85-89.

T.L. Webster, J.B. Murphy, J.C. Gosse, L. Spooner. 2006. The application of LiDAR-derived digital elevation model analysis to geological mapping: an example from the Fundy Basin, Nova Scotia, Canada. Can. J. of Remote Sensing, 32, 2, 173–193.

N.H. Woodcock, M. Fischer. 1986. Strike-slip duplexes. J. of Struct. Geol., 8, 7, 725-735.

A.P. Young, S.A. Ashford. 2006. Application of airborne LiDAR for seacliff volumetric change and beach-sediment budget contributions J. of Coastal Res., 22, 2, 307-318.

Figure captions

Figure 1. Geological features of the Leon metamorphic domain (LMD). a. Location of the LMD within the granitic and shear zone patterns in the Armorican Variscides. b. Sketch geological map of the LMD. The map of the offshore studied area is drawn from Lefort (1977) and Chauris and Hallegouet (1989). NASZ, NOSZ, PGSZ, PNSZ, North Armorican, North Ouessant, Pospoder-Guissény, and Pierres Noires shear zones, respectively. The white star corresponds to the sample location of the dated St-Renan granite. c. A-B synthetic structural cross-section, location on Fig. 1b (modified according to Ballèvre et al., 2009).

Figure 2. Location map of geophysical records and seafloor rock sampling in the Molene archipelago. LiDAR flight lines and sonar echosounder surveys are drawn. Map location on Fig. 1.

Figure 3. 5 m-resolution bathymetric map of the Molene archipelago obtained from merging LiDAR and swath data. Boxes indicate the location of structural fabrics discussed in the text and shown in Fig. 6 (left columns). Emerged lands are in black. Colored circles are the location of *in-situ* seafloor rock samples. Lithology and microstructures of a number of representative samples are shown in thin sections (cv22, cv24, cv32, cv29, cv10, p11, cv2). Amph., amphibole; Biot., biotite; Chl., chlorite; Fk., k-feldspar; Musc., muscovite; Plag., plagioclase; Qtz., quartz. cv24, cv29 and cv2 are XZ sections (perpendicular to foliation and parallel to the stretching lineation) in strained rocks; S. foliation, C. shear plane. Lx mag., magmatic lineation in p11. cv8 is a rock sample. Black circles correspond to the location of onshore structures used to calibrate the interpretation of bathymetric fabrics (see Fig. 6, right columns).

Figure 4. Offshore geological map of the Leon Variscan basement in the Molène archipelago and trace of structural lineaments, established from alti-bathymetric data and seafloor rock sample lithology (x52 data) (structural interpretation in the text).

Figure 5. Concordia diagrams of the dated igneous rocks: a. and b. Tera-Wasserburg plots of analysed zircons from the St-Renan granite; c. U-Th/Pb plot of analysed monazites from the St-Renan granite; d. Conventional Concordia plot of analysed zircons from the Groac'h Zu intrusive complex. Individual error ellipses and Concordia ages are given at the 2-sigma level. MSWD stands for Mean Square Weighted Deviation, and N is the number of analyses used for the calculation of the Concordia age.

Figure 6. Shaded relief images of fabrics extracted from the digital elevation model of the Molene archipelago seafloor (LiDAR and echo sounder records) (left column), and onshore corresponding structures (right column); locations as boxes and black circles in Fig. 3. a. NNE-SSW fracture network in the Aber Idult granite (fabric 'a'); b. NW-SE magmatic lineation in the Aber Ildut granite (fabric 'b'); c. Regional foliation, as expressed in the Le Conquet micaschists (fabric 'c'); d. Shear zones (fabric 'd'), (d1a, d1b, sinistral and dextral shear zones with C/S structures, respectively; d2a, Sinistral C/S ductile fabric in the Lesneven orthogneisses; d2b, Dextrally sheared pegmatitic dykelet in the St-Renan granite within the NASZ; e. Curved magmatic fabric in the Groac'h Zu intrusion (fabric 'e'). S, schistosity, C, shear plane.

Figure 7. Detailed structural and geological map of the SW Léon coastal zone from the Corsen to St Mathieu Points (Location in Fig. 3). Dotted line corresponds to an inferred large-scale post-foliation fold.

Figure 8. Main structural features along the Corsen-St Mathieu cross-section. a. Attitude of stretching lineations (89 plunge data) and foliations (91 dip data). b. 3D-block-diagrams summarizing the geometry and kinematics of the dominant ductile strains within the different structural domains along the transect. Greyish faces correspond to field structures illustrated on Fig. 8c. c. Ductile strain observed in the field. c1, Sigmoidal quartz lens indicating top-to-the-NE reverse shear in the Le Conquet micaschists; c2, Early structures, related to the top-to-the-NE reverse shear (regional schistosity and asymmetrical folds), dissected by top-to-the-SW dextral-normal shear surfaces (Le Conquet gneiss facies); c3, Rotated garnets with asymmetric pressure-shadows indicating dextral-normal shearing. An early schistosity (S1) is fossilized within the porphyroblasts (Le Conquet micaschists); c4, SW-plunging stretching lineation (Lm, pressure-shadows on garnets) associated with dextral-normal shearing; c5, Pure dextral shear recorded by C/S-type fabrics in orthogneiss (Brest Fm.) along the PNSZ; c6, Shallowly-plunging lineation (Lm, Q-Fk corrugated surfaces) associated with dextral strike-slip shear (same formation).

Figure 9. Foliation trajectory map (including magmatic fabrics and ductile shear zones) extrapolated from the lineament map. BSZ, FSZ, GZSZ, NASZ, NMSZ, and PNSZ; Beniguet, Fromveur, Groac'h Zu, North Armorican, North Molene, and Pierres Noires shear zones.

Figure 10. Focused views of the 5m-resolution alti-bathymetric map at the eastern extremity of the Groac'h Zu intrusive complex. a-b. Shaded-relief image and structural interpretation of the sheared southern margin of the Groac'h Zu intrusion. Green, black, red thin, and dark bold blue lines correspond, respectively, to magmatic fabrics, regional schistosity (S), shear planes

(C) associated to dextral shear zones (red bold lines), and sinistral shear zones. Abbreviations as in Fig. 9. c. Anomalous trend of the regional foliation in a disturbance faulted (sinistral) zone. S, regional schistosity. d. Asymmetric folds and coeval shear planes post-dating the regional schistosity. e. Cross-cutting relationships between the regional foliation (early) and later shear surfaces in the BSZ.

Figure 11. Kinematic model of the southern part of the LMD during the ~320 Ma dextral shearing event and coeval intrusions. The overall dextral shear zone pattern is interpreted as a linked system dominated by the NASZ (north) and PNSZ (south), and their (duplex) overlapping domain. Inset shows the trace of the Monts d'Arrée (MASZ) and Montagnes Noires (MNSZ) dextral shear zones throughout the Central Armorican Domain (after Darboux and Le Gall, 1986, modified). Abbreviations as in Figs. 1 and 9.

Table 1: Characteristics of the remote sensing dataset used to produce a single DEM of the studied offshore area.

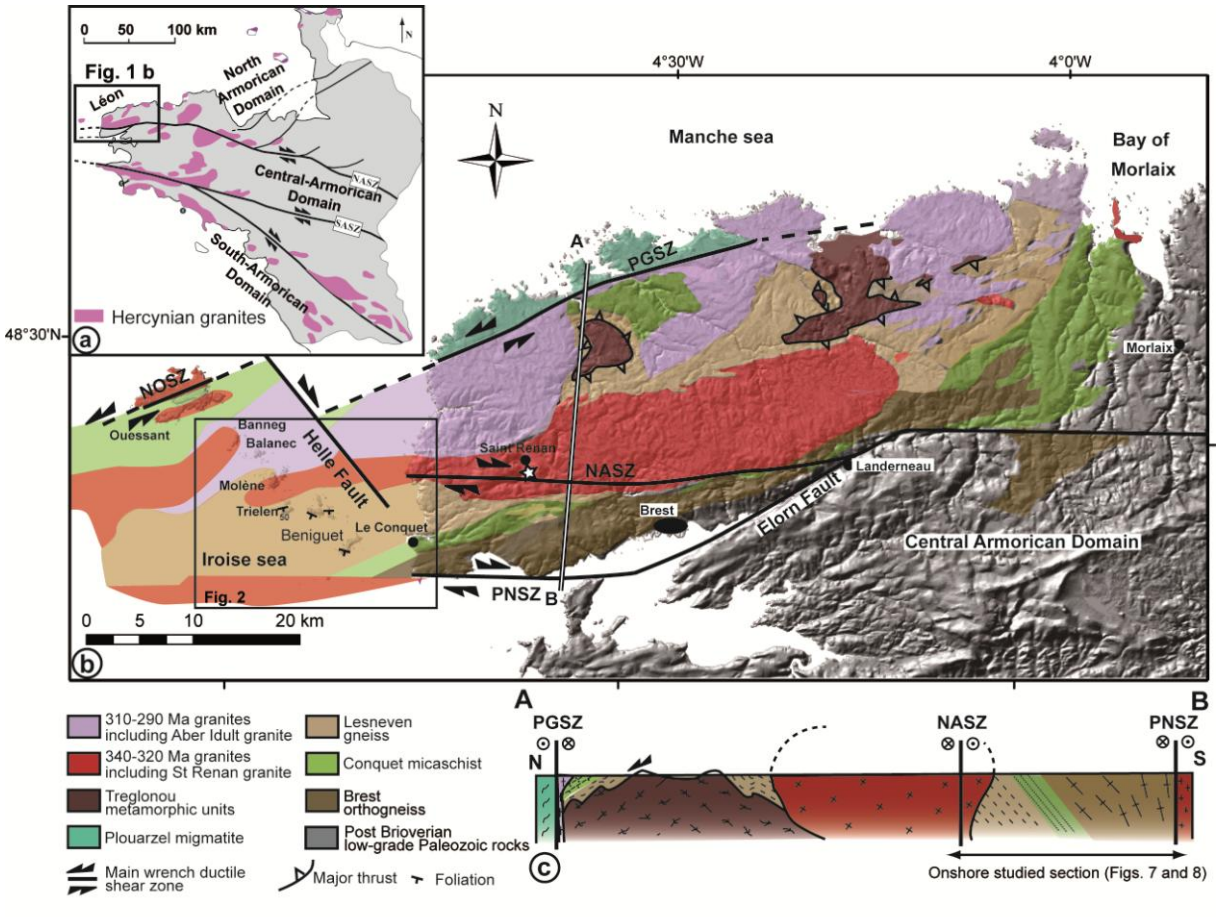

Figure 1

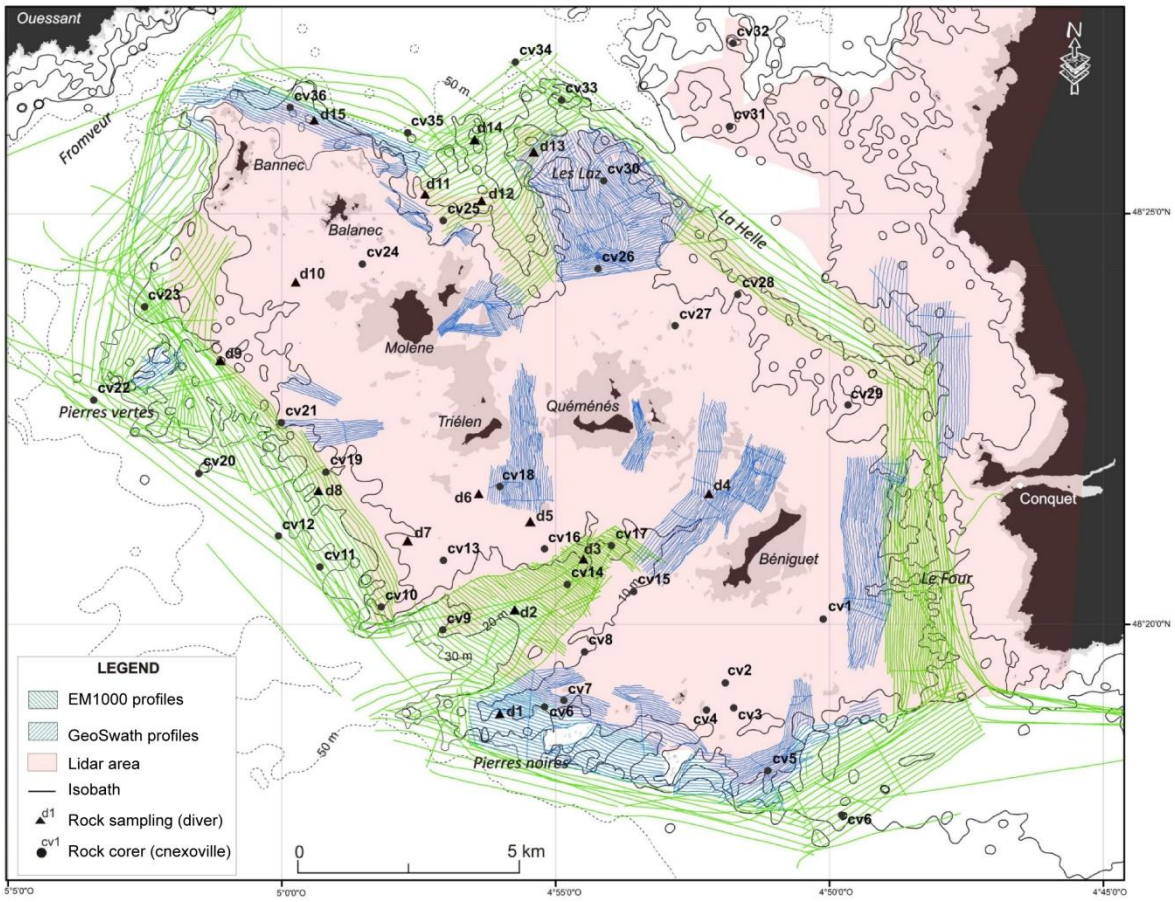

Figure 2

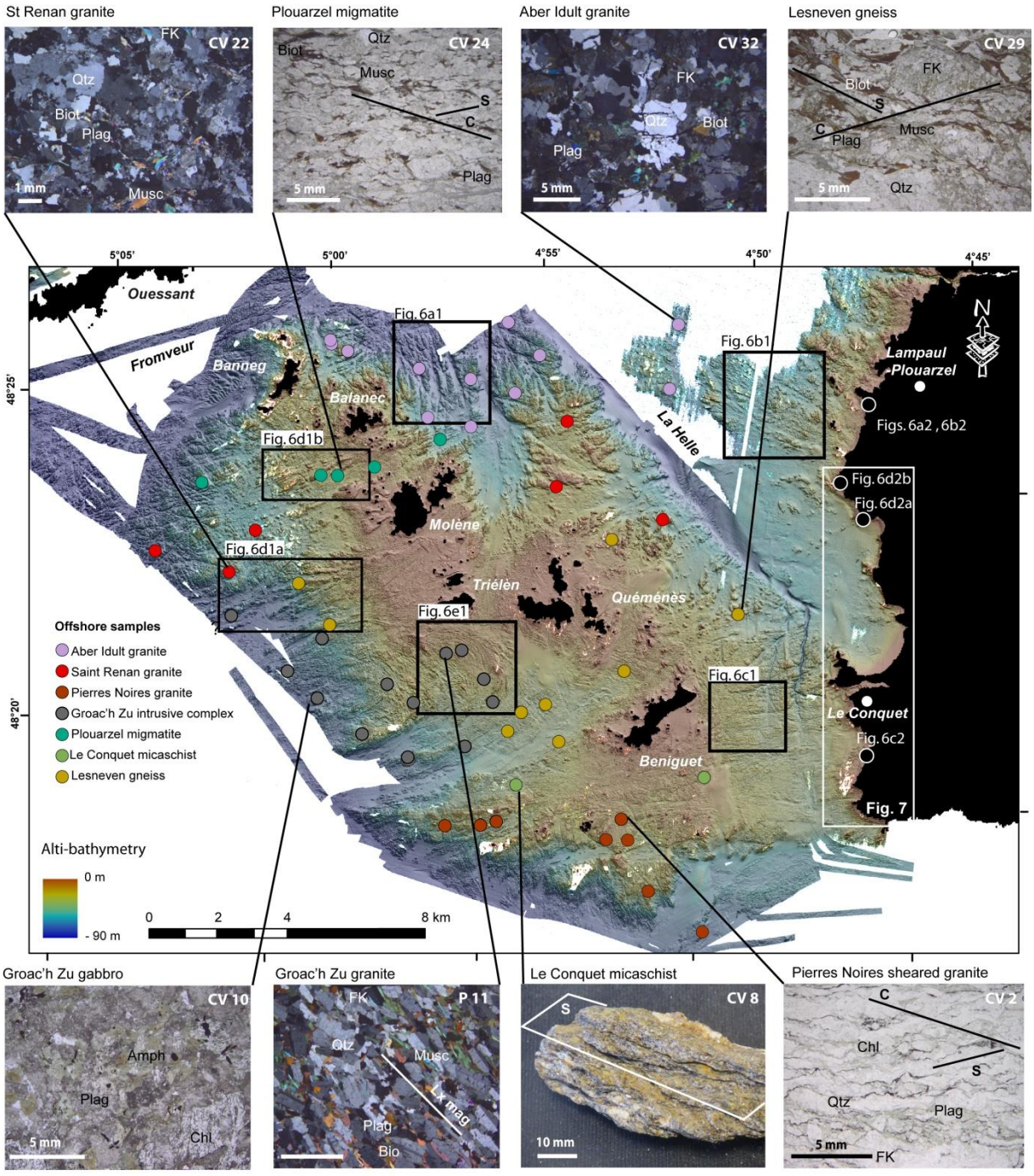

Figure 3

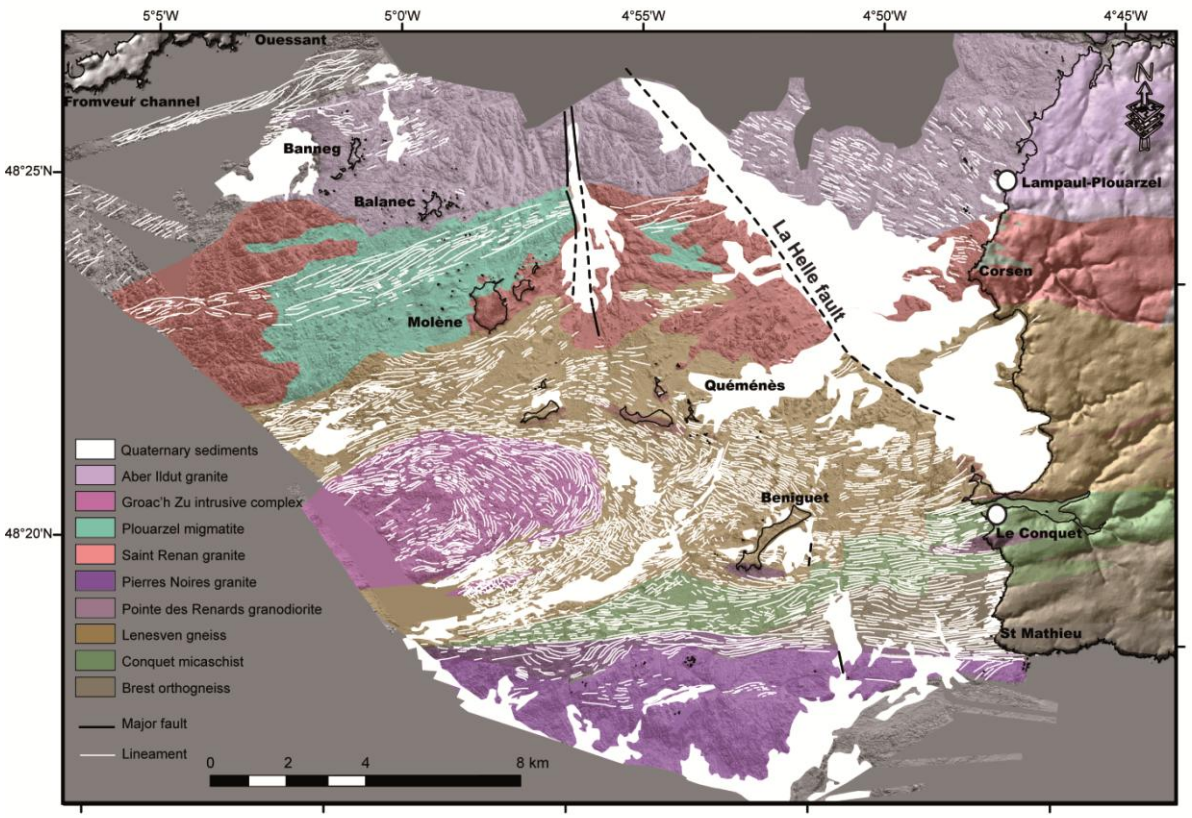

Figure 4

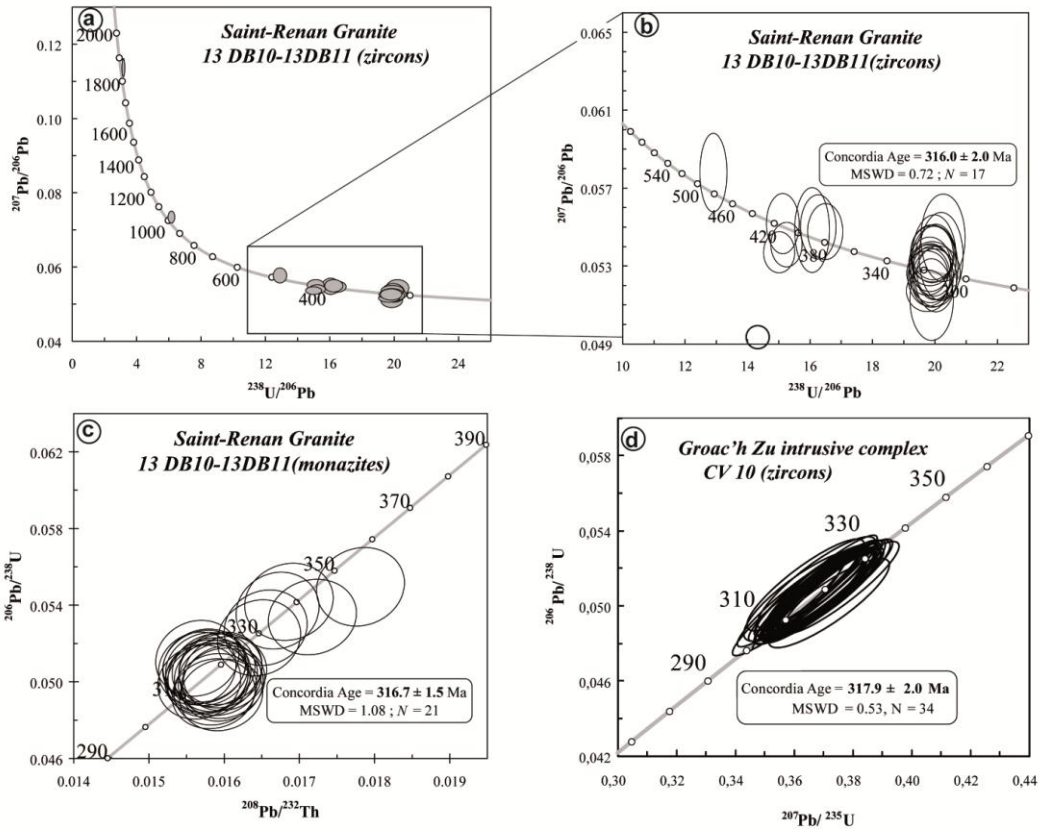

Figure 5

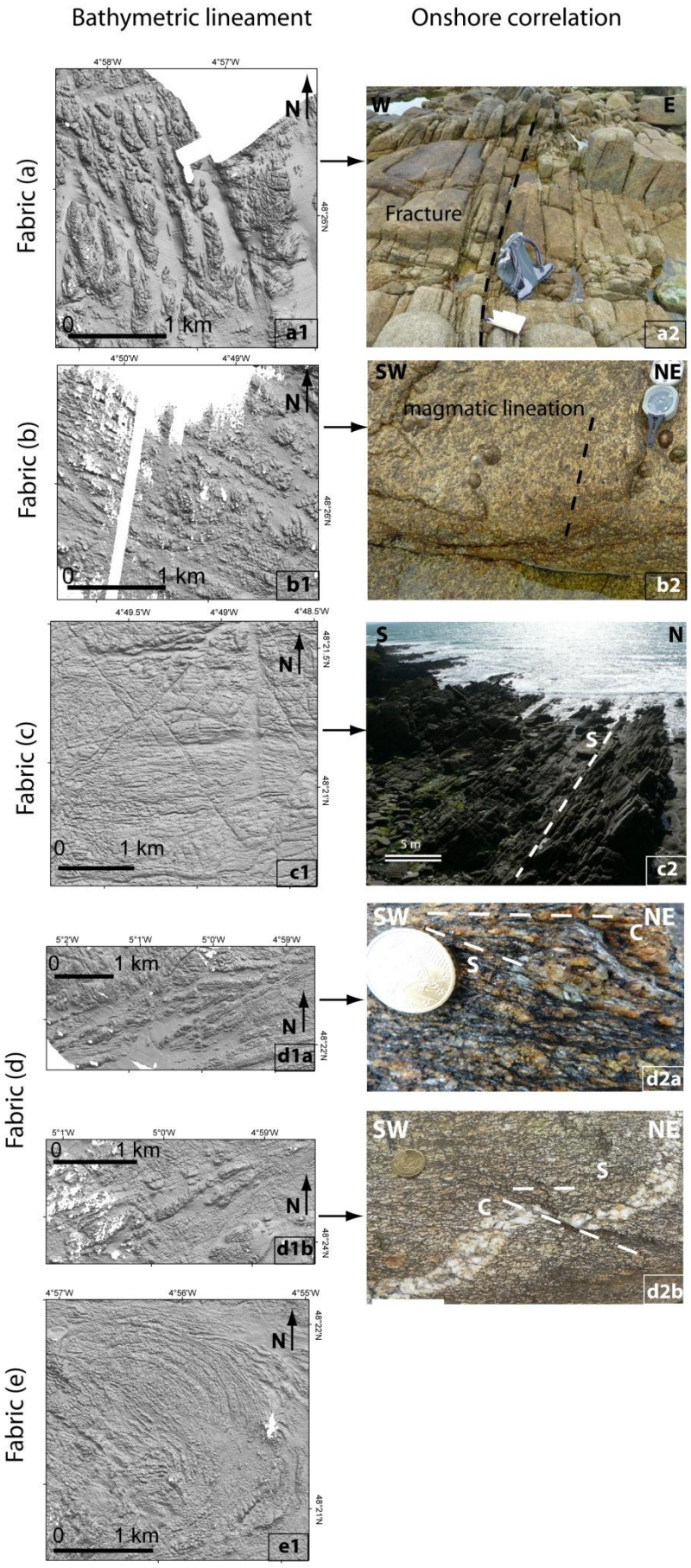

Figure 6

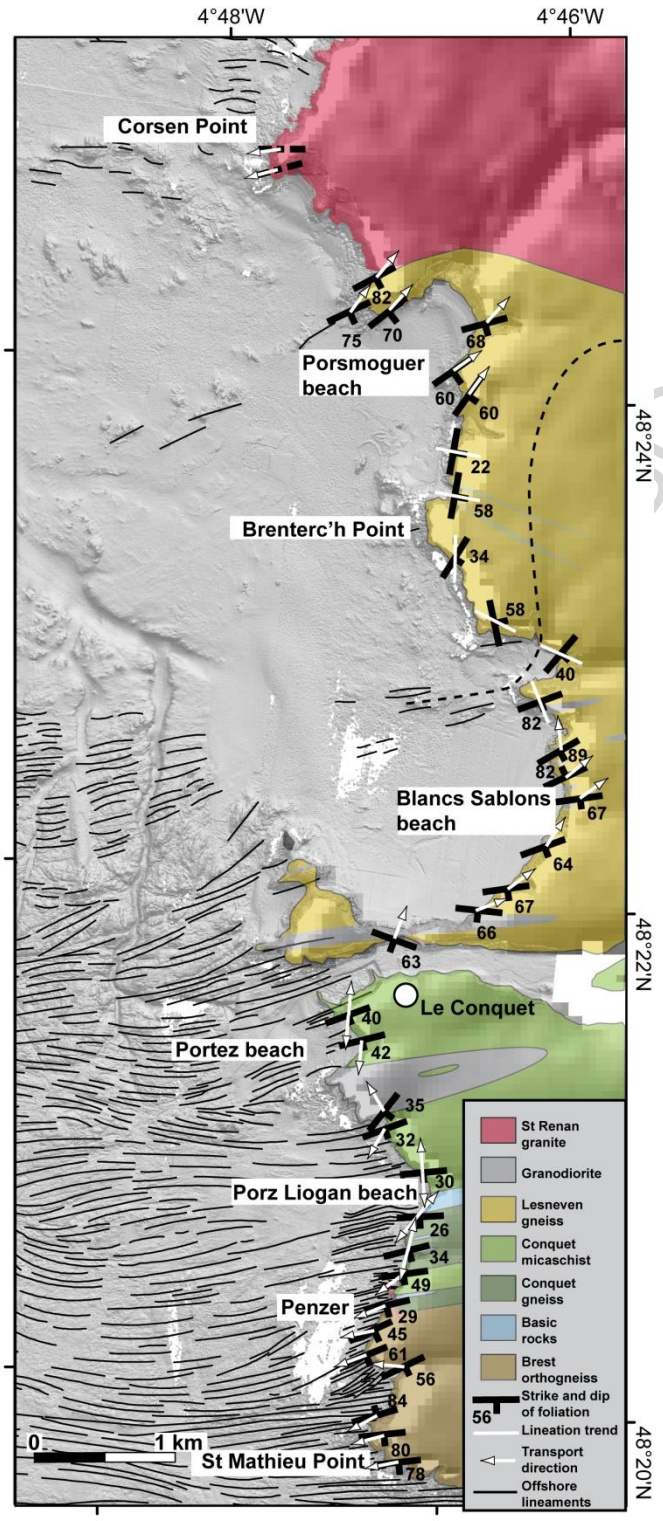

Figure 7

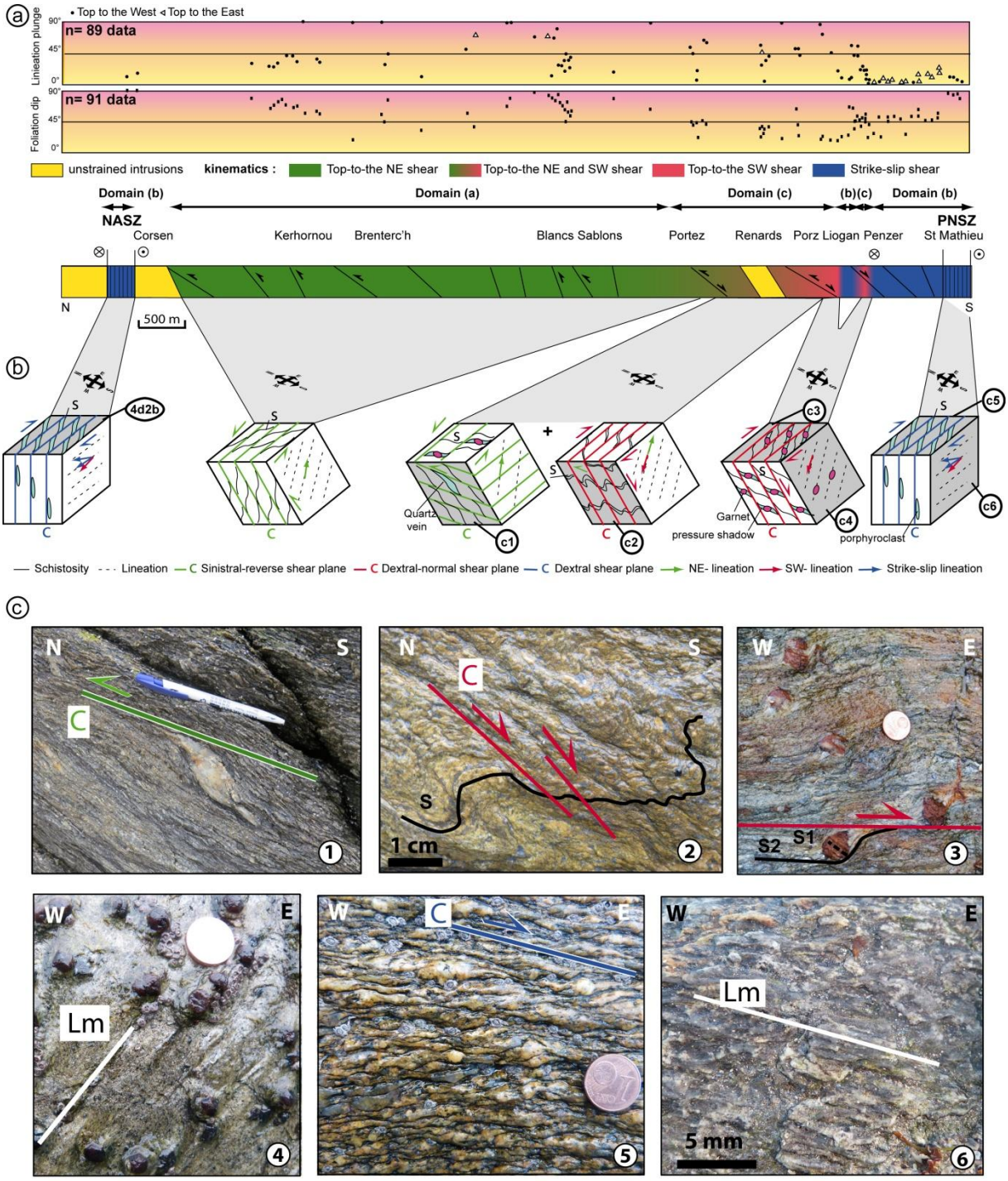
a
• Top to the West ◃ Top to the East
Lineation plunge
Foliation dip
n= 89 data
n= 91 data
unstrained intrusions
kinematics :
Top-to-the NE shear
Top-to-the NE and SW shear
Top-to-the SW shear
Strike-slip shear
Domain (b)
NASZ
Domain (a)
Domain (c)
(b)(c)
Domain (b)
PNSZ
Corsen
Kerhornou
Brenterc'h
Blancs Sablons
Portez
Renards
Porz Liogan
Penzer
St Mathieu
N
S
500 m
b
4d2b
Quartz vein
c1
c2
c3
Garnet
pressure shadow
c4
porphyroclast
c5
c6
Schistosity
Lineation
Sinistral-reverse shear plane
Dextral-normal shear plane
Dextral shear plane
NE- lineation
SW- lineation
Strike-slip lineation
c
1
2
1 cm
3
S1
S2
4
Lm
5
6
5 mm

Figure 8

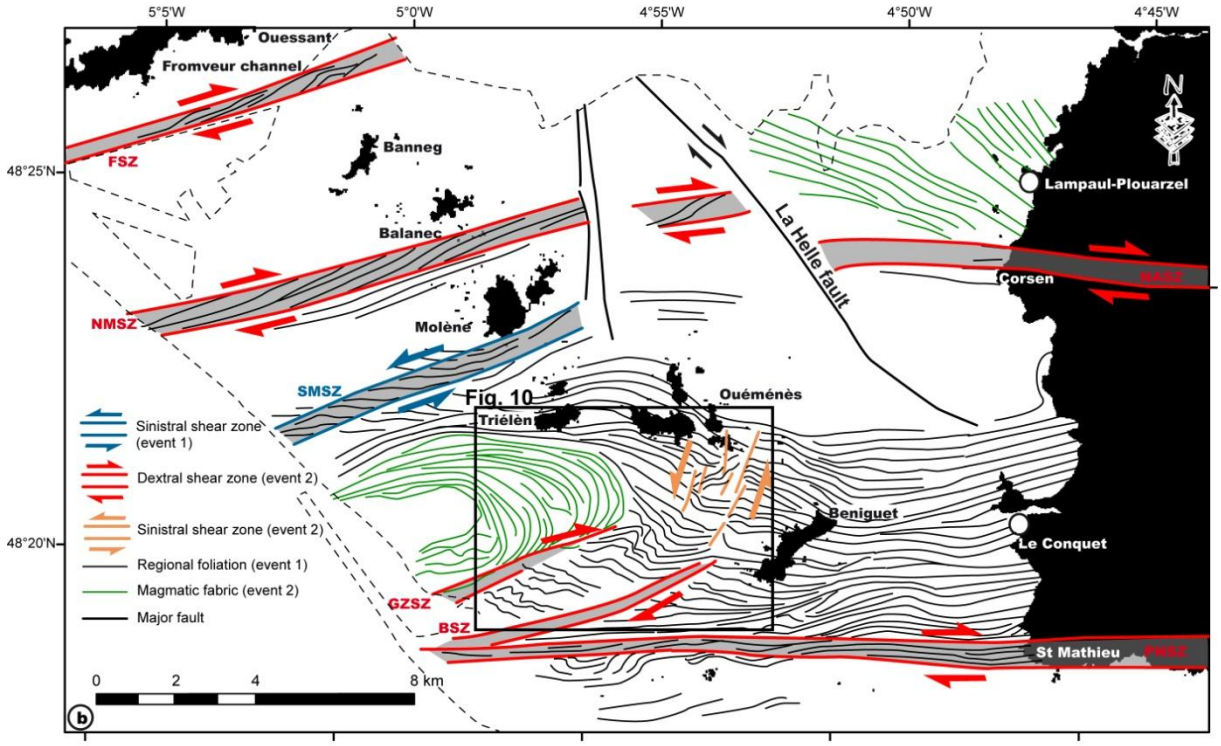

Figure 9

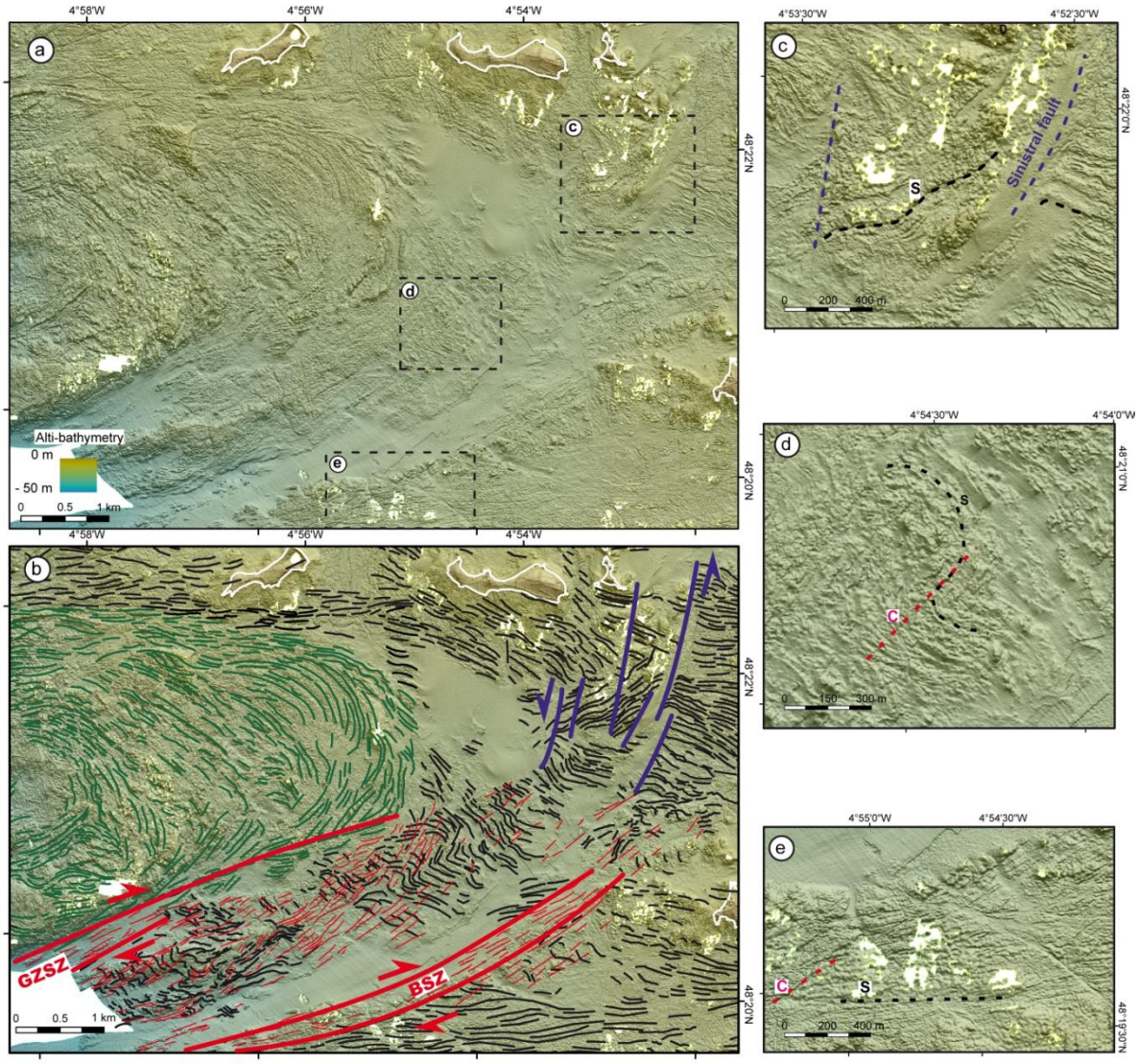

Figure 10

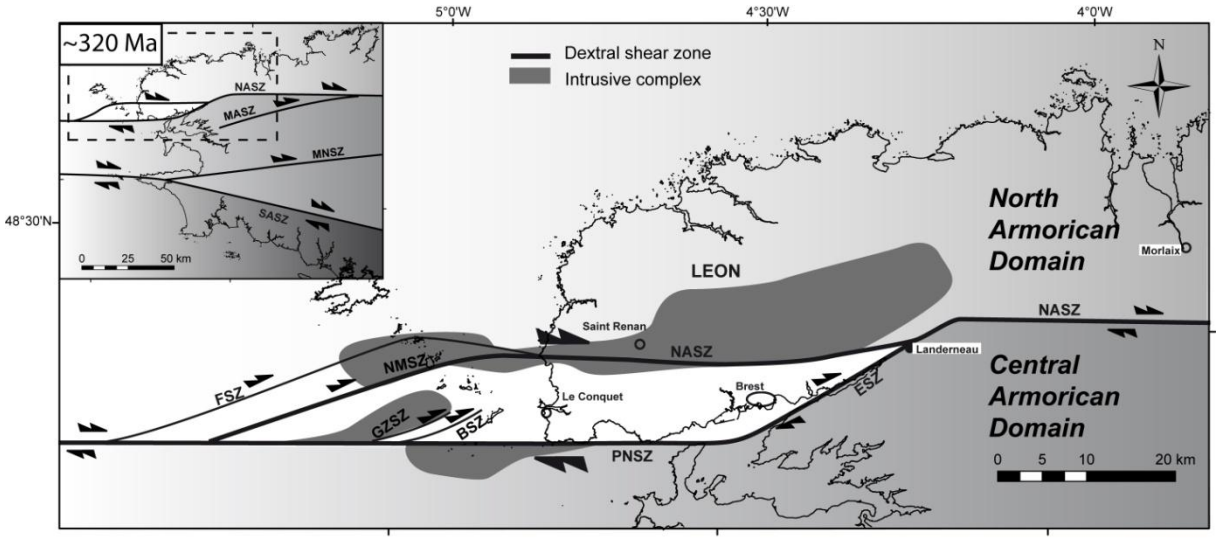

Figure 11

	Type of equipment	Date of survey acquisition	Surface area	Maximum depth range	DEM resolution
Airborne LiDAR bathymetry	Haw keye Mk II	04-05/2010	170 km^2	+27 / -32 m	5 m
Multibeam echosounder	Simrad EM1000 100 kHz	05-06/2011	97 km^2	-3 / -97 m	2 m
Interferometric sonar bathymetry	GeoSwath Plus 250 kHz	09/2010 05/2011 09/2011	54 km^2	+2 / -62 m	50 cm

Table 1: Characteristics of remote sensing dataset used to produce a single DEM of the studied offshore area